# A semianalytical three-dimensional process-based model for hyporheic nitrogen dynamics in gravel bed rivers

Alessandra Marzadri,[1] Daniele Tonina,[2] and Alberto Bellin[1]

Received 21 February 2011; revised 30 September 2011; accepted 4 October 2011; published 17 November 2011.

[1] We present a three-dimensional semianalytical process-based model of dissolved oxygen and dissolved inorganic nitrogen (DIN) transformation within the hyporheic zone of gravel bed rivers. Oxygen and multispecies solute transport is solved within a Lagrangian framework with transformation of DIN species modeled by linearized Monod's kinetics, with temperature-dependent reaction rate coefficients derived from field experiments. Our solutions, which are obtained under the assumptions of sediments with uniform hydraulic properties and negligible local dispersion, highlight the importance of morphological characteristics of the streambed on DIN transformations within the hyporheic zone. By means of this model we explore the effects of streambed topography and relative abundance of ammonium and nitrate in stream waters on the reactive nitrogen cycle in the hyporheic zone of gravel bed rivers with a pool and riffle morphology. Our model shows complex concentration dynamics within the hyporheic zone that may act as a source or a sink of nitrogen depending on the residence time distribution, which can be parameterized in terms of streambed morphology, and the ratio between the in-stream concentrations of ammonium and nitrate. Application of the model to seven natural streams shows good agreement between predicted and measured nitrous oxide emissions from their hyporheic zone.

**Citation:** Marzadri, A., D. Tonina, and A. Bellin (2011), A semianalytical three-dimensional process-based model for hyporheic nitrogen dynamics in gravel bed rivers, *Water Resour. Res., 47*, W11518, doi:10.1029/2011WR010583.

## 1. Introduction

[2] Nitrogen is a ubiquitous element essential for organism metabolism. In aquatic systems, it is commonly found in the form of dissolved inorganic nitrogen (DIN), which includes ammonium ($NH_4^+$), nitrate ($NO_3^-$), and nitrite ($NO_2^-$), three reactive nitrogen ($N_r$) species produced by the decay of organic matter and added by fertilizers [*Galloway et al.*, 2004, 2008]. With the introduction of the Haber-Bosch process at the beginning of the twentieth century and the following burst of agricultural productivity in the so-called green revolution [*Smil*, 1999], human activities have increased $N_r$ availability in natural systems, which would be otherwise nitrogen limited, leading to eutrophication and impaired habitat quality [*Cooper*, 1993]. Today, many streams flowing in agricultural and urban areas suffer from the impact of excessive nitrogen inputs under the form of ammonium and nitrate [*Spalding and Exner*, 1993], supplemented by atmospheric deposition, which is the dominant distribution pathway at the global scale [*Galloway et al.*, 2008]. Nitrite is a less common species of DIN, and its contribution can be expressed in terms of nitrate [*Tesoriero et al.*, 2000].

[3] Under aerobic conditions, nitrifying bacteria oxidize $NH_4^+$ to $NO_2^-$ and then to $NO_3^-$. On the other hand, under anaerobic conditions and in the presence of electron donors, such as dissolved organic carbon (DOC), denitrifying heterotrophic bacteria reduce $NO_3^-$ to nitrogen gases $N_{gas}$ under the form of both nitrous oxide ($N_2O$), and molecular nitrogen ($N_2$) [see, e.g., *Shaffer et al.*, 2001]. Therefore, the increased availability of $N_r$ triggers larger emissions of $N_{gas}$ from terrestrial ecosystems with respect to the situation in the previously undisturbed conditions. Recent estimates suggest that rivers, estuaries, and continental shelves contribute approximately with 30% of the total global $N_2O$ emissions [*Seitzinger et al.*, 2000], and the share from rivers is produced mainly within the hyporheic zone (HZ) because in this saturated environment the concentration of dissolved oxygen (DO) is lower than in stream waters [*Hemond and Duran*, 1989; *Beaulieu et al.*, 2011].

[4] Because aerobic bacteria consume DO to sustain nitrification and respiration processes, the hyporheic environment becomes increasingly reduced along any flow path from downwelling to upwelling zones (Figure 1). As DO decreases to a given threshold, denitrification starts removing nitrate. Consequently, both nitrification and denitrification processes may take place within the streambed sediments according to oxygen dynamics [see, e.g., *Triska et al.*, 1993; *Sheibley et al.*, 2003; *Krause et al.*, 2009].

[5] Our understanding of hyporheic exchange has improved considerably in the last few years, and models evolved from the transient storage model [*Bencala and*

[1]Department of Civil and Environmental Engineering, University of Trento, Trento, Italy.
[2]Center for Ecohydraulics Research, University of Idaho, Boise, Idaho, USA.


0043-1397/11/2011WR010583

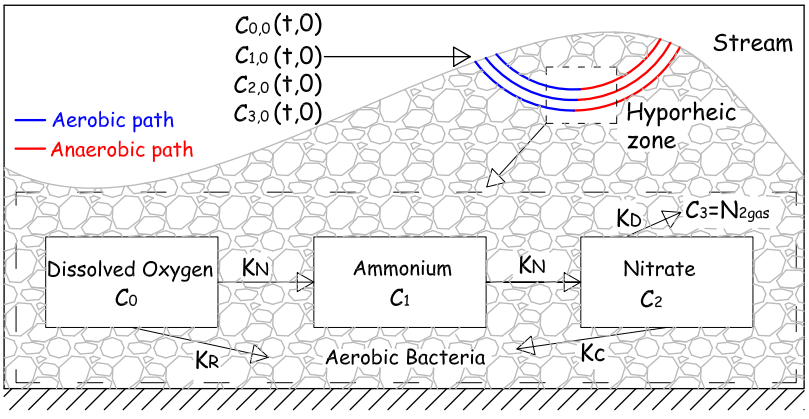


**Figure 1.** Simplified sketch of the nitrogen cycle within the hyporheic zone (HZ). $C_0$ indicates dissolved oxygen (DO) concentration, $C_1$ is the concentration of ammonium, $C_2$ is the concentration of nitrate, $C_3$ is the concentration of nitrogen gas, $K_R$ is the reaction rate of biomass respiration, $K_N$ is the reaction rate of nitrification, $K_D$ is the reaction rate of denitrification, and $K_C$ is the reaction rate of biomass consumption.

*Walters*, 1983], which idealizes the hyporheic exchange as a mean flow rate into a well-mixed HZ of constant volume, to more sophisticated travel time models [see, e.g., *Stonedahl et al.*, 2010; *Marzadri et al.*, 2010, and references therein]. Despite these developments most modeling studies on DIN dynamics use a simplified description of the hyporheic exchange [see, e.g., *Rutherford et al.*, 1995; *Packman and Bencala*, 2000; *Hantush*, 2007] or empirical relations between in-stream DIN concentrations and their transformations [see, e.g., *Newbold et al.*, 2000; *Mulholland and DeAngelis*, 2000]. These models have the merit of including biotic processes but neglect the spatial variability of hyporheic flows caused by streambed topography and its control on redox conditions and biogeochemical processes as evidenced in a number of experimental studies [e.g., *Harvey and Bencala*, 1993; *Triska et al.*, 1993; *Huttel et al.*, 1996; *Wondzell and Swanson*, 1996; *Elliott and Brooks*, 1997; *Duff and Triska*, 2000; *Packman and Brooks*, 2001; *Marion et al.*, 2002; *Tonina and Buffington*, 2007]. Another line of attack is to use computational fluid dynamics to model in detail the complexity arising from coupling transport with biogeochemical processes [*Cardenas et al.*, 2008], but alternative and less costly approaches are needed when dealing with applications and interpretation of experimental data since collecting all the information needed to run such models is difficult, if not impossible.

[6] A more attractive approach is writing a transport equation in Lagrangian (travel time) coordinates [see, e.g., *Dagan et al.*, 1992], which in the absence of transverse local dispersion allows reducing the dimensionality of the transport problem while maintaining flow dimensionality. This approach has been used by *Boano et al.* [2010] to solve numerically the coupled transport and biogeochemical models of DIN dynamics in the intrameander HZ under the hypothesis that the flow field can be approximated as horizontal (two-dimensional). In the present work we adopt the same approach but consider a fully three-dimensional flow field and obtain analytical solutions, instead of numerical solutions, of the coupled transport and biogeochemical models based on the characterization of the travel time distribution within the HZ.

[7] Our goal is to develop a process-based framework to predict the fate of nitrogen within the HZ and quantify the effects of hyporheic processes on in-stream nitrogen loads from morphodynamic and hydraulic characteristics of the stream. In addition, we show the flexibility of our modeling framework by applying it to predict $N_2O$ emissions measured by *Beaulieu et al.* [2008] in seven headwater streams within the Kalamazoo River basin in southwestern Michigan, United States.

## 2. Method

### 2.1. Hyporheic Flow

[8] Let us consider a stationary flow field in alluvial sediments characterized by a homogeneous and isotropic hydraulic conductivity $K$. Mass conservation leads to the following governing equation:

$$\frac{\partial^2 h}{\partial x^2}+\frac{\partial^2 h}{\partial y^2}+\frac{\partial^2 h}{\partial z^2}=0, \tag{1}$$

which in conjunction with Darcy's law [*Freeze and Cherry*, 1979],

$$\mathbf{u}=[u,v,w]=-\frac{K}{\vartheta}\nabla h, \tag{2}$$

allows computing the flow velocity field $\mathbf{u}$ after imposing suitable boundary conditions. In equations (1) and (2), $\vartheta$ is the sediment porosity, which we assume to be spatially constant, and $h$ is the piezometric head.

[9] Recently, *Marzadri et al.* [2010] presented the analytical solutions of equations (1) and (2) in a computational domain delimited by six planar boundaries with impervious

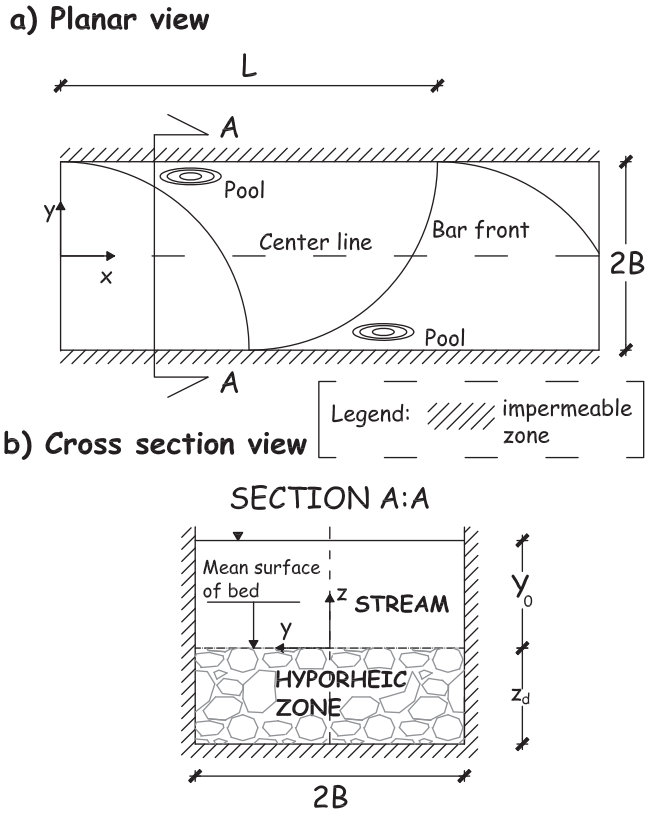


**Figure 2.** Sketch of the streambed topography with the reference coordinate system located along the centerline of the channel (modified from *Marzadri et al.* [2010]). The coordinates $x$, $y$, and $z$ are positive downstream, leftward, and upward, respectively: (a) planar view and (b) cross-section view of the channel, where $2B$ is the channel width, $Y_0$ is the mean flow depth, $L$ is the bar length, and $z_d$ is the alluvium depth.

conditions at both the domain's bottom and lateral planes (stream banks) and imposed constant heads at the upstream and downstream planes, so as to obtain a head drop equal to the streambed drop between them (see Figure 2). Furthermore, the spatially variable head provided by the solution of *Colombini et al.* [1987] for streams with alternate bars in equilibrium with the flow regime was imposed at the stream sediment interface, which was approximated with the mean bed elevation. The analytical solutions were obtained under the further hypotheses of steady state flow conditions, i.e., constant water discharge, and fully submerged bars [*Marzadri et al.*, 2010]. In more complex systems, such as those described by *Cardenas and Wilson* [2007] and *Hantush* [2005], the above solutions can be generalized by varying the boundary conditions to account for the effects of ambient groundwater gradients and the exchange with river banks and the riparian zone.

[10] A comparative study of nitrogen export from headwater streams through North America showed that ammonium entering these streams was removed after short distances, while the removal of nitrate occurred after distances 5–10 times longer were traveled in longer streams [*Peterson et al.*, 2001]. Similarly, in a heavily instrumented gravel bar of the Drift Creek, Marion County, Oregon, United States, *Zarnetske et al.* [2011] showed that net nitrification occurred in zones characterized by short residence times, while net denitrification was predominant in zones with comparatively longer residence times. In light of this experimental evidence, we focus our analysis on the following two cases: a small, steep (S) stream 2.6 m wide, with a slope of 1.32% and a water discharge of 0.177 $m^3 s^{-1}$, representative of a class of headwater streams with the HZ in prevailing aerobic conditions, and a large, low-gradient stream (L) 26 m wide, with a slope of 0.13% and a water discharge of 17.759 $m^3 s^{-1}$, representative of streams with a significant portion of the HZ in anaerobic conditions. These geometries are within the range reported by *Rutherford* [1994, Table 4.2], who summarizes the characteristics of some of the most important rivers of the world. As shown by *Marzadri et al.* [2010], the hyporheic residence times of these streams differ by orders of magnitude. In Table 1, we report the hydraulic and morphodynamic parameters of these two representative streams.

### 2.2. Transport Model

[11] Under the assumption that local dispersion is negligible compared to advection [*Dagan*, 1989; *Rubin*, 2003], the governing equation for transport of reacting solutes is

$$R_i \frac{\partial C_i}{\partial t} + \mathbf{u} \cdot \nabla C_i = f_i, \quad i = 0, 1, 2, 3, \tag{3}$$

where $C_i$ is the concentration of the $i$th species and $R_i$ and $f_i$ are the retardation coefficients and the reaction rates for dissolved oxygen ($i = 0$), ammonium ($NH_4^+, i = 1$), nitrates ($NO_3^-, i = 2$), and nitrogen gases (sum of $N_2O$ and $N_2$, $i = 3$), respectively. Hereafter, the concentration of the $N_r$ species is expressed as nitrogen equivalent. Of all the above species only $NH_4^+$ is significantly influenced by sorption, therefore in the present work we assume $R_0 = R_2 = R_3 = 1$ and $R_1 = R \geq 1$ [see, e.g., *Hemond and Duran*, 1989; *Triska et al.*, 1994; *Duff and Triska*, 2000; *Bernot and Dodds*, 2005].

[12] A suitable variable transformation allows writing equation (3) in the following more manageable form [*Shapiro and Cvetkovic*, 1988; *Dagan et al.*, 1992; *Cvetkovic and Dagan*, 1994]:

$$R_i \frac{\partial C_i}{\partial t} + \frac{\partial C_i}{\partial \tau} = f_i, \tag{4}$$

where the space coordinates $\mathbf{x} = (x_1, x_2, x_3)$ are replaced with the travel time $\tau$ of a particle moving along a streamline, which is defined as

$$\tau(\mathbf{a}) = \int_0^{l(\tau;\mathbf{a})} \frac{\mathrm{d}\xi}{|\mathbf{u}(\xi)|}. \tag{5}$$

In equation (5), $|\mathbf{u}(\xi)|$ is the magnitude of the velocity vector at the position $\mathbf{x} = \xi$, and $l$ is the distance measured

**Table 1.** Hydraulic and Morphodynamic Parameters for the Small, Steep Stream (S) and the Large, Low-Gradient Stream (L)[a]

| Stream | $B$ (m) | $z_d$ (m) | $Y_0$ (m) | $L$ (m) | $s_0$ (%) | $d_{50}$ (m) | $Q$ ($m^3\ s^{-1}$) | $\beta$ | $\theta$ | $d_S$ | $H^*_{BM}$ |
|---|---|---|---|---|---|---|---|---|---|---|---|
| S | 1.3 | 2.6 | 0.1 | 16.92 | 1.32 | 0.01 | 0.177 | 13 | 0.08 | 0.1 | 2.0338 |
| L | 13 | 26 | 1 | 163.14 | 0.13 | 0.01 | 17.759 | 13 | 0.08 | 0.01 | 0.5756 |

[a]Here $2B$ is the channel width, $z_d$ is the alluvium depth, $Y_0$ is the mean flow depth, $L$ is the bar length, $s_0$ is the stream slope, $d_{50}$ is the median grain size, $Q$ is the stream discharge, $\beta$ is the aspect ratio, $\theta$ is the Shields number, $d_S$ is the relative submergence, and $H^*_{BM}$ is the dimensionless bar amplitude.

along the streamline from the injection point **a** to the position that the particle assumes at time $t = \tau$. Notice that according to this Lagrangian scheme, $\tau = 0$ identifies the position **a** where the streamline originates within the downwelling area, $A_{dw}$.

### 2.3. Biogeochemical Model

[13] In order to simplify as much as possible the biogeochemical model and focus on the most relevant processes we introduce a number of simplifications, which are generally valid in most gravel bed rivers with hyporheic sediments containing low organic matter. In most of these rivers the carbon to nitrogen ratio is in the range $20 \leq C{:}N \leq 30$, and water temperature is below 20°C. Under these conditions, mineralization and immobilization are small to negligible, although in equilibrium [*Lewis et al.*, 2007]. The additional assumptions that pH is constant and dissolved organic carbon (DOC) is not a limiting factor for biomass, which is assumed to be in equilibrium with equal rates of growth and death, allow considering only the dynamics of inorganic nitrogen species and the associated DO dynamic. This is justified by the observation that in the HZ of gravel bed rivers, DO depletes faster than DOC [*Zarnetske et al.*, 2011] such that the only ambient factors affecting biomass activity are temperature and DO concentrations. For settings in which DOC is a limiting factor, our modeling approach can be generalized by adding an equation describing DOC consumption during both nitrification and denitrification and its feedback on biomass activity. Under these conditions, biomass consumes only nitrate along the aerobic part of the streamlines [*Sobczak et al.*, 2003; *Potter et al.*, 2010].

[14] Furthermore, we neglect both dissimilatory nitrate reduction to ammonium (DNRA) and anaerobic ammonium oxidation (ANAMMOX). Although DNRA, which back transforms nitrate in ammonium, was observed in soils [*Sylvia et al.*, 2005] and in streams with a C:N ratio larger than 30 [*Tiedje*, 1988], it is currently believed to be a minor factor in most stream settings [*Kelso et al.*, 1999; *Duff and Triska*, 2000; *Puckett et al.*, 2008]. Very little is known regarding the occurrence of ANAMMOX during the anaerobic oxidation of $NH_4^+$ to $N_2O$ in surface waters, but it is also believed to be of secondary importance [*Kendall et al.*, 2007].

[15] Under these simplifying assumptions, we obtain the simplified conceptual model of the processes controlling the transformation of DIN species within the hyporheic sediments shown in Figure 1. Ammonium ($NH_4^+$) is oxidized to nitrate ($NO_3^-$) by nitrifying bacteria, whereas nitrate ($NO_3^-$) shows a more complex dynamic with denitrification that in addition to producing $N_{gas}$, contrasts the tendency of increasing $NO_3^-$ concentration through nitrification.

[16] DO concentration $C_0$ regulates ambient conditions as aerobic or anaerobic and, consequently, the chemical processes occurring within the sediments [e.g., *Hantush*, 2007]. In general, $C_0$ varies with water temperature, salinity, and stream aeration. For well-aerated and low-salinity streams, a situation typically observed in gravel bed streams, $C_0$ is approximately 10 mg $L^{-1}$ at a stream temperature of 15°C, but it reduces at higher temperatures. When DO concentrations fall below a given threshold, the system shifts from aerobic to anaerobic conditions. Field-scale experiments indicate that this threshold is in the range 2–4 mg $L^{-1}$ [*Bölke and Denver*, 1995]. As discussed by *Green et al.* [2010], these values are larger than those observed in batch experiments, with the difference accounting for the upscaling from core to field scale of an inherently heterogeneous process.

[17] Here we assume that once DO concentration reaches the threshold value of $C_{0,lim} = 4$ mg $L^{-1}$, microbial respiration is inhibited, and consequently, DO is no longer depleted. However, different site-specific values of this threshold can be set in the model if environmental conditions suggest that.

[18] We consider first the solution for the DO concentration because of its regulating effect on the dynamics of the $N_r$ species. The behavior of $C_0$ within the HZ can be obtained by solving equation (4) specialized for $i = 0$ with $R_0 = 1$ and the following reaction term:

$$f_0 = -K_{RN} C_0, \tag{6}$$

where $K_{RN} = K_R + K_N$ is a rate coefficient that cumulates the effects of biomass respiration and nitrification. Initial and boundary conditions are $C_0(\tau, 0) = C_{0,lim}$ and $C_0(0, t) = C_{0,s}$, respectively, where $C_{0,s}$ is the initial concentration of dissolved oxygen in the stream water.

[19] Under these conditions, the solution for dissolved oxygen concentrations along a streamline assumes the following form:

$$C_0(\tau, t) = C_{0,s}\, e^{-K_{RN}\tau}\, H(t-\tau) + C_{0,lim}\, e^{-K_{RN}t}\, [1 - H(t-\tau)], \tag{7}$$

where $H(t)$ is the Heaviside step function. Notice that hereafter, for simplicity of notation, we omit indicating the dependence of $\tau$ from **a**. According to equation (7), streamlines are in aerobic conditions from the downwelling area ($\tau = 0$) to the position along the streamline where $C_0 = C_{0,lim}$. This position can be computed by solving equation

(7) for $\tau$ under the condition that $C_0(\tau_{\lim}, t = \tau_{\lim}) = C_{0,\lim}$:

$$\tau_{\lim} = \frac{1}{K_{RN}} \ln\left(\frac{C_{0,s}}{C_{0,\lim}}\right). \quad (8)$$

The remaining portion of the streamline, i.e., for $\tau > \tau_{\lim}$, is in anaerobic conditions. It is important to note that $\tau_{\lim}$ depends on dissolved oxygen concentrations in the stream, but it is independent from the initial condition $(C_0(\tau, 0))$ within the hyporheic sediment. According to our simplified scheme, $C_0$ declines exponentially, at a rate $K_{RN}$, in the aerobic portion of the streamline, which is identified with the condition $\tau \leq \tau_{\lim}$, while it is constant and equal to $C_{0,\lim}$ in the remaining of the streamline, which is then in anaerobic conditions.

[20] Once the behavior of $C_0$ is known, the dynamics of the $N_r$ species can be obtained by solving equation (4), specialized for $i = 1, 2, 3$, and with the following linear Monod kinetics:

$$\begin{aligned} f_1(\tau, t) &= -K_N(\tau) C_1(\tau, t), \\ f_2(\tau, t) &= K_N(\tau) C_1(\tau, t) - [K_C(\tau) + K_D(\tau)] C_2(\tau, t), \\ f_3(\tau, t) &= K_D(\tau) C_2(\tau, t), \end{aligned} \quad (9)$$

where $K_N$, $K_C$, and $K_D$ are the nitrification, biomass uptake due to microbial assimilatory reduction of nitrate, and denitrification rate coefficients, respectively. Equations (9) are obtained from the nonlinear Monod equations under the assumption that the concentrations of the $N_r$ species are much smaller than the corresponding half saturation constant [*Bailey and Ollis*, 1977]. This approximation is applicable to most rivers even if impacted by agricultural and other $N_r$ releasing human activities [*McLaren*, 1976; *Cooper*, 1984; *Sheibley et al.*, 2003; *Buss et al.*, 2005; *Kjellin et al.*, 2007; *Basu et al.*, 2010].

[21] These parameters vary with dissolved oxygen concentrations and therefore with $\tau$, reflecting the fact that both nitrification and biomass uptake stop when oxygen concentrations reach $C_{0,\lim}$, while denitrification is inhibited when $C_0 > C_{0,\lim}$. Note that according to our simplified biogeochemical model, $C_0$ cannot be reduced below $C_{0,\lim}$ because all the processes consuming oxygen become inactive when $C_0 = C_{0,\lim}$. We will return later on to this point when discussing the dynamics of the three DIN species within the HZ (see section 3.3).

[22] The above reaction parameters depend on water temperature through the Arrhenius equation:

$$K_j = K_j^{(20)} \varphi_j^{T-20}; \quad j = R, N, C, D, \quad (10)$$

where $T$ is the hyporheic water temperature, which for simplicity we assume to be spatially constant within the HZ, $K_j^{(20)}$ are the rate coefficients for the $j$th reaction at 20°C, and $\varphi_j$ are dimensionless temperature coefficients (values assigned to these coefficients are reported in Table 5).

[23] We consider now the behavior of $N_r$ species starting with the solution of equation (4) specialized for $NH_4^+$, which for a well-mixed in-stream $NH_4^+$ concentration $C_1(0, t) = C_{1,0}(t)$ assumes the following form [*van Genuchten*, 1981]:

$$C_1(\tau, t) = \begin{cases} C_{1,0}(t - R\,\tau)\, \chi_1(\tau), & t \geq R\,\tau, \\ 0, & t < R\,\tau, \end{cases} \quad (11)$$

with

$$\chi_1(\tau) = \exp\{-K_N\, \tau[1 - H(\tau - \tau_{\lim})] - K_N\, \tau_{\lim} H(\tau - \tau_{\lim})\}, \quad (12)$$

where sorption of ammonium is modeled by a linear equilibrium kinetic, which leads to a constant retardation factor $R_1 = R \geq 1$.

[24] We turn now to $NO_3^-$. According to our simplified model, the nitrate dynamic within the HZ is regulated by equation (4) with $i = 2$, supplemented by the biogeochemical model (9), and the well-mixed in-stream $NO_3^-$ concentration $C_2(0, t) = C_{2,0}(t)$ as a boundary condition. The initial condition is zero $NO_3^-$ concentration within the HZ, i.e., $C_2(\tau, t = 0) = 0$. Furthermore, in line with experimental evidence [see, e.g., *Bernot and Dodds*, 2005], we assume that nitrates are not affected by sorption, such that $R_2 = 1$. Under these assumptions the solution of equation (4), specialized for $i = 2$, reads

$$C_2(\tau, t) = \begin{cases} C_{2,0}(t - \tau)\, \chi_{2,2}(\tau) + \int_0^t C_{1,0}(t - t')\, \chi_{2,1}(\tau, t')\, \mathrm{d}t', & t \geq \tau, \\ 0, & t < \tau, \end{cases} \quad (13)$$

where the kernel functions $\chi_{2,2}$ and $\chi_{2,1}$ are given by

$$\chi_{2,2}(\tau) = \exp[(K_C - K_D)(\tau - \tau_{\lim}) H(\tau - \tau_{\lim}) - K_C\, \tau] \quad (14)$$

$$\chi_{2,1}(\tau, t) = \begin{cases} \dfrac{K_N}{R-1} e^{\left(\frac{K_N - RK_C}{R-1}\right)\tau} e^{\left(\frac{K_C - K_N}{R-1}\right)t} [H(t - \tau) - H(t - R\,\tau)], & \tau \leq \tau_{\lim}, \\ \dfrac{K_N}{R-1} e^{\frac{K_N - K_C}{R-1}(\tau - t)}\, e^{-K_D(\tau - \tau_{\lim}) - K_C\, \tau_{\lim}} \{H(t - \tau) - H[t - \tau - (R-1)\, \tau_{\lim}]\}, & \tau > \tau_{\lim}. \end{cases} \quad (15)$$

[25] Consistent with the adopted biogeochemical model, these solutions for $C_1$ and $C_2$ have been obtained by assuming that the reaction rates vary along the streamline depending on the local redox conditions. In the aerobic portion of the streamline ($\tau \le \tau_{\lim}$), $K_C$ and $K_N$ are both constant and larger than zero, while $K_D = 0$. Conversely, $K_D$ is constant and larger than zero, while $K_N = K_C = 0$, in the anaerobic portion of the streamlines ($\tau > \tau_{\lim}$).

[26] If sorption of ammonium is also negligible, such that $R_1 = R = 1$, the kernel function (15) reduces to

$$\chi_{2,1}(\tau) = \frac{K_N}{K_C - K_N}\left(e^{-K_N\tau + K_N(\tau-\tau_{\lim})H(\tau-\tau_{\lim})} - e^{(K_C-K_D)(\tau-\tau_{\lim})H(\tau-\tau_{\lim})-K_C\tau}\right). \quad (16)$$

Cases in which this approximation is possible are discussed by *Butturini et al.* [2000]. Finally, we obtain the concentration of $N_{gas}$ (i.e., the sum of $N_2$ and $N_2O$) produced along the streamline by solving equation (4) specialized for $i = 3$ with $R_3 = 1$. The resulting equation is applied to the anaerobic portion of the streamlines because we assume that denitrification is the only process producing $N_{gas}$.

[27] With the initial condition of zero concentration within the HZ, i.e., $C_3(\tau, 0) = 0$, and a well-mixed concentration in the stream water, i.e., $C_3(t, 0) = C_{3,0}(t)$, the solution of the equation (4) with $i = 3$ assumes the following form:

$$C_3(\tau,t) = \begin{cases} C_{3,0}(t-\tau) + K_D\int_{\tau_{\lim}}^{\tau} C_2(\tau', t-\tau+\tau')\mathrm{d}\tau', & \tau > \tau_{\lim}, \quad t \ge \tau, \\ C_{3,0}(t-\tau), & \tau < \tau_{\lim}, \quad t \ge \tau, \end{cases} \quad (17)$$

while $C_3(\tau, t) = C_3(\tau, 0) = 0$ for $t < \tau$. For nonsorbing ammonium (i.e., for $R_1 = R = 1$), equation (17) reduces to

$$C_3(\tau,t) = \begin{cases} C_{3,0}(t-\tau) + \dfrac{K_D[1-\chi_{2,2}(\tau)]}{K_C+K_D} C_{2,0}(t-\tau) \\ \qquad + \dfrac{K_D[1-\chi_1(\tau)]}{K_C+K_D-K_N} C_{1,0}(t-\tau), & t \ge \tau, \\ 0, & t < \tau. \end{cases} \quad (18)$$

[28] The behavior of $C_1$, as given by equation (11), is an attenuated translation of the input signal $C_{1,0}(t)$, with an attenuation that becomes constant and independent from $\tau$ in the anaerobic portion of the streamline ($\tau > \tau_{\lim}$) when nitrification stops and $NH_4^+$ is not consumed further. Note that the position at which $\tau = \tau_{\lim}$ changes with the streamline.

[29] The concentration of $NO_3^-$ is more complex and assumes the form of a convolution of the streamflow concentration of both $NH_4^+$ and $NO_3^-$ with suitable kernel functions. The convolution reduces to a multiplication when $NH_4^+$ can be considered to be a nonsorbing solute, as with the other $N_r$ species.

[30] Finally, the concentration $C_3$ of $N_{gas}$ is simply the translation of the well-mixed in-stream concentration $C_{3,0}(t)$ for $\tau < \tau_{\lim}$ (i.e., in the aerobic portion of the streamline) and a function of $C_2$ for $\tau > \tau_{\lim}$, which reflects the emissions due to denitrification.

### 2.4. Solution of the Transport Model

[31] Once the concentration $C_i(\tau, t)$ is known for $i = 1, 2, 3$, along the streamlines, the total mass flux of the $i$th species through the upwelling area can be computed through

$$\begin{aligned} Q_{M,i}(t) &= \int_{A_{up}} \vartheta\, u(\boldsymbol{\xi})\, C_i[\tau_{up}(\mathbf{a}), t]\, \mathrm{d}A(\boldsymbol{\xi}) \\ &= \int_{A_{dw}} \vartheta u(\mathbf{a})\, C_i[\tau_{up}(\mathbf{a}), t]\, \mathrm{d}A(\mathbf{a}), \\ i &= 0, 1, 2, 3, \end{aligned} \quad (19)$$

where $\tau_{up}(\mathbf{a})$ is the time a particle spends traveling from the position $\mathbf{x} = \mathbf{a}$ within the downwelling area $A_{dw}$ to the position $\mathbf{x} = \boldsymbol{\xi}$, where it exits from the upwelling area $A_{up}$. In addition, $\mathrm{d}A(\mathbf{a})$ and $\mathrm{d}A(\boldsymbol{\xi})$ are the infinitesimal cross-section areas of the streamline at $\mathbf{x} = \mathbf{a}$ and $\mathbf{x} = \boldsymbol{\xi}$, respectively. Equation (19) is written by taking advantage of the continuity equation along the streamline connecting $\mathbf{a}$ to $\boldsymbol{\xi}$, $\vartheta\, u(\mathbf{a})\, \mathrm{d}A(\mathbf{a}) = \vartheta\, u(\boldsymbol{\xi})\, \mathrm{d}A(\boldsymbol{\xi})$, and the result that flux and resident concentrations coincide in the absence of pore-scale dispersion [*Kreft and Zuber*, 1978; *Demmy et al.*, 1999].

[32] Another important quantity is the mean flux concentration through the upwelling area, which is defined as the ratio between the mass flux given by expression (19) and water discharge, $Q = \int_{A_{dw}} \vartheta\, u(\mathbf{a})\, \mathrm{d}A(\mathbf{a})$, through both downwelling and upwelling areas:

$$C_{F,i}(t) = \frac{Q_{M,i}(t)}{Q}, \quad i = 1, 2, 3. \quad (20)$$

The flux concentration of the three $N_r$ species given by equation (20) represents the response of the HZ of a single morphological unit to stream nutrient loads and provides a tool to study in-stream nutrients cycling at the watershed scale as a process in a sequence along the stream network. The function $C_{F,i}(t)$ embeds the interplay between biogeochemical processes and the residence time within the HZ, which is controlled by streambed morphology, flow regime, and sediment hydraulic properties.

[33] Another quantity of interest is the mass of the $i$th species that at time $t$ is within the HZ, which is given by

$$M_i(t) = \int_{A_{dw}} \vartheta\, u(\mathbf{a}) \int_0^{\tau_{up}(\mathbf{a})} C_i[\tau, t]\, \mathrm{d}\tau\, \mathrm{d}A(\mathbf{a}), \quad i = 1, 2, 3. \quad (21)$$

## 3. Results and Discussion

### 3.1. Validation With Field Experiments

[34] We apply our model to a unique data set that includes stream morphodynamic characteristics, stream DIN and DO concentrations, and $N_2O$ emissions from the HZ of 12 mixed sand-gravel low-gradient streams within the Kalamazoo River basin in southwestern Michigan, United States [*Beaulieu et al.*, 2008, 2009].

[35] We computed the morpho-hydrodynamic parameters shown in Table 2 by using the information reported in the work by *Beaulieu et al.* [2008]. In particular, we computed

**Table 2.** Hydrodynamics and Morphodynamic Parameters Used in the Simulations of Seven Streams Within the Kalamazoo River Basin in Southwestern Michigan, United States

| Site | Stream | $Q^a$ (L s$^{-1}$) | $Y_0{}^a$ (m) | $v^a$ (m s$^{-1}$) | $B$ (m) | $\beta$ | $\theta$ | $d_S$ | $d_{50}$ (m) | $s_0$ (%) | $K$ (m s$^{-1}$) |
|---|---|---|---|---|---|---|---|---|---|---|---|
| A1 | Axtell | 32.6 | 0.073 | 0.113 | 1.97 | 26.99 | 0.044 | 0.137 | 0.01 | 1.0 | 0.001 |
| A2 | Tannery | 8.7 | 0.126 | 0.027 | 1.30 | 10.27 | 0.076 | 0.079 | 0.01 | 1.0 | 0.001 |
| A3 | Bullet | 4.0 | 0.06 | 0.067 | 0.50 | 8.29 | 0.036 | 0.167 | 0.01 | 1.0 | 0.001 |
| A4 | Arcadia | 62.7 | 0.106 | 0.162 | 1.83 | 17.26 | 0.064 | 0.094 | 0.01 | 1.0 | 0.001 |
| A5 | Urbandale | 37.9 | 0.142 | 0.143 | 0.93 | 6.56 | 0.086 | 0.070 | 0.01 | 1.0 | 0.001 |
| A6 | Spring Brook | 16.9 | 0.091 | 0.13 | 0.72 | 7.85 | 0.055 | 0.110 | 0.01 | 1.0 | 0.001 |
| A8 | Allegan | 21.9 | 0.091 | 0.102 | 1.18 | 13.01 | 0.055 | 0.110 | 0.01 | 1.0 | 0.001 |

[a]Reported by *Beaulieu et al.* [2008, Table 1].

$\beta = Q/(2vY_0^2)$, where $Q$ is water discharge, $v$ is the mean stream velocity, and $Y_0$ is the water depth, by using the data of *Beaulieu et al.* [2008, Table 1] and estimated $\theta = s_0/(1.65\ d_s)$ and $d_s = d_{50}/Y_0$ by assuming $s_0 = 1.0\%$ and $d_{50} = 1$ cm, according to the general description of the sites reported in the same study. The analysis is limited to 7 out of 12 streams, for which the observed morphodynamic parameters ($\beta$, $\theta$, $d_s$, and $d_{50}$) are within the range of applicability of the morphodynamical model [*Marzadri et al.*, 2010].

[36] In-stream DIN concentrations and biogeochemical parameters are taken from *Beaulieu et al.* [2008, Tables 1 and 3, 2009, Table 4], while DO concentration in stream water was obtained from *Arango and Tank* [2008, Table 2]. Moreover, since there is no information about $K_C$, we used one tenth of the value reported by *Dent and Henry* [1999] for $T = 6$°C. We return later on this point to better explain and justify our choice (see section 3.2). Finally, we considered in-steam DIN concentrations to be constant in time and extended the simulations up to the time needed to reach steady state conditions in the flux concentrations of DIN species emerging from the upwelling area. Table 3 summarizes these biogeochemical parameters and the values adopted for $C_{0,\mathrm{lim}}$, the reaction rate of biomass respiration, and the reaction rate of biomass uptake.

[37] Figure 3 shows the comparison of ($N_2O$) production measured and predicted with our model in the seven mixed gravel-sand streams [*Beaulieu et al.*, 2008, 2009]. Model results match the observed values well, with some large errors in streams 3 and 6. The disagreement between model and experimental data could be due to measurement and derived coefficient uncertainty and to soil characteristics (hydraulic conductivity and porosity), which we derived from the literature. Another possible source of error is the assumption that alternate bar theory applies to all seven streams considered in the present study. The fact that our model was able to predict with minimal error $N_2O$ production in seven streams without any fitting is a promising result, showing that our model can be used to assess DIN dynamics in the HZ of gravel bed rivers.

### 3.2. Transformation Conditions of DIN Species

[38] Although we developed our model for time-variable in-stream $N_r$ concentrations, we discuss here the case of an instantaneous pulse injection of ammonium and nitrate. Given the structure of equations (11)–(18), this assumption allows elucidating and discussing the interplay between the residence time $\tau_{\mathrm{up}}$ within the HZ and biogeochemical processes in shaping the response of the river reach to the nutrient load. Furthermore, we assume $R = 1$ with the motivation that in gravel bed rivers sorption of ammonium is often negligible [*Butturini et al.*, 2000] and again that given the structure of the solutions, considering $R > 1$ does not add insights into the study of the dynamics of the $N_r$ species, which are chiefly controlled by redox conditions.

[39] With these premises and after substituting into equation (21) the expressions of $C_i(\tau, t)$ given by equations (11)–(18), specialized for the case of instantaneous injection of $NH_4^+$ and $NO_3^-$, i.e., $C_{i,0}(t) = C_{i,0}\ \delta(t)\ \Delta t$, with $\Delta t \to 0$, for $i = 1, 2$ and $C_{3,0}(t) = 0$, we obtain the following expressions for the dimensionless mass of the $i$th $N_r$ species that is within the HZ at time $t$:

$$\mu^*_{M,i}(t) = \frac{\chi_i(t)\ C^*_{i,0}}{Q} \int_{A_{\mathrm{dw}}} u(\mathbf{a})\, H\left[\tau_{\mathrm{up}}(\mathbf{a}) - t\right] \mathrm{d}A(\mathbf{a}), \quad i = 1, 2, 3, \tag{22}$$

**Table 3.** Biogeochemical Parameters Used in the Simulations of Seven Streams Within the Kalamazoo River Basin in Southwestern Michigan, United States[a]

| Site | $C_{0,0}{}^b$ (mg L$^{-1}$) | $C_{0,\mathrm{lim}}$ (mg L$^{-1}$) | $C_{1,0}{}^c$ (μg L$^{-1}$) | $C_{2,0}{}^c$ (mg L$^{-1}$) | $C_{3,0}{}^c$ (μg L$^{-1}$) | $K_R$ (d$^{-1}$) | $K_N{}^d$ (d$^{-1}$) | $K_D{}^d$ (d$^{-1}$) | $K_C{}^e$ (d$^{-1}$) | $N_2O$ Yield[f] (%) |
|---|---|---|---|---|---|---|---|---|---|---|
| A1 | 7.3 | 3 | 83 | 0.18 | 0.42 | 0.053 | 9.903 | 2.922 | 0.523 | 0.9 |
| A2 | 7.3 | 3 | 72 | 0.13 | 0.52 | 0.053 | 2.116 | 1.319 | 0.523 | 6.9 |
| A3 | 10 | 3 | 5 | 0.38 | 0.73 | 0.053 | 48.571 | 1.854 | 0.523 | 8.4 |
| A4 | 9.4 | 3 | 46 | 1.08 | 0.91 | 0.053 | 7.383 | 0.482 | 0.523 | 6.3 |
| A5 | 8.6 | 3 | 47 | 0.33 | 0.45 | 0.053 | 9.350 | 1.075 | 0.523 | 2.3 |
| A6 | 9.5 | 3 | 7 | 0.69 | 0.67 | 0.053 | 33.909 | 0.344 | 0.523 | 10.8 |
| A8 | 9.9 | 3 | 19 | 1.65 | 0.75 | 0.053 | 4.587 | 0.096 | 0.523 | 21.1 |

[a]$C_{3,0}$ is the concentration of $N_{\mathrm{gas}}(0,t) = N_2(0,t) + N_2O(0,t)$, with $N_2(0,t) = 0$ and $N_2O$ yield = [$N_2O$ production rate/denitrification rate] × 100.
[b]Reported by *Arango and Tank* [2008, Table 2].
[c]Reported by *Beaulieu et al.* [2008, Table 1].
[d]Reported by *Beaulieu et al.* [2008, Table 4].
[e]One tenth of the value reported by *Dent and Henry* [1999] for $T = 6$°C.
[f]Reported by *Beaulieu et al.* [2009, Table 3].

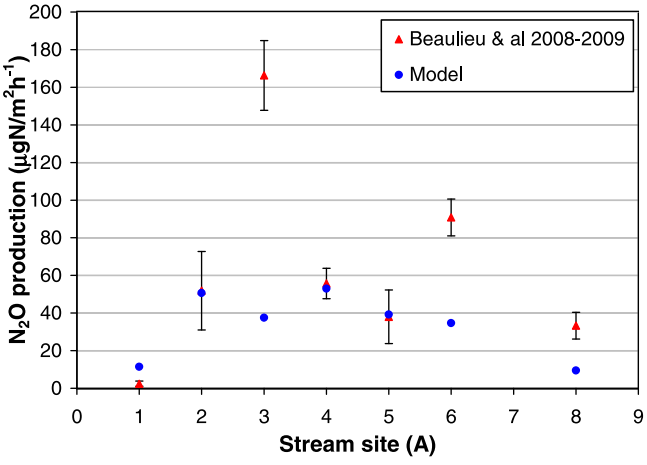


**Figure 3.** Comparison between the production per unit area of nitrous oxide predicted with the model and published by *Beaulieu et al.* [2008, 2009].

where $C^*_{i,0} = C_{i,0}/\mathrm{DIN}_0$, $i = 1, 2$, with $\mathrm{DIN}_0 = C_{1,0} + C_{2,0}$ representing the total in-stream DIN concentration, and

$$\chi_2(t) = \mathrm{RC}\,\chi_{2,1}(t) + \chi_{2,2}(t), \tag{23}$$

$$\chi_3(t) = \left\{\frac{K_D[1-\chi_{22}(t)]}{(K_C+K_D)\,\mathrm{RC}} + \frac{K_D[1-\chi_1(t)]}{K_C+K_D-K_N}\right\} H[t-\tau_{\mathrm{lim}}], \tag{24}$$

where RC is the ratio between in-stream ammonium and nitrate concentrations ($\mathrm{RC} = C_{1,0}/C_{2,0}$).

[40] Table 4 shows the in-stream water DIN concentrations, and Table 5 reports the parameters of the biogeochemical model. Simulations are conducted at the constant water temperature of 6°C, which represents a typical winter situation. Since, to the best of our knowledge, no specific values of $K_C$ are available in literature for the HZ of gravel bed rivers, in our simulations we used one tenth of the value provided by *Dent and Henry* [1999] for a streambed colonized by the peryphiton community (algae and bacteria) under the hypothesis that $K_C$ is by nine tenths due to the activity of this community, which does not colonize the HZ (see Table 5). To all the other parameters of the biogeochemical model reported in Table 5, we assigned values within the range of values observed in gravel bed rivers under conditions similar to those adopted in the present work.

**Table 4.** Initial In-stream Concentrations of Dissolved Oxygen and Nitrogen Species[a]

| Test | $C_{0,0}$[b] (mg $L^{-1}$) | $C_{1,0}$[c] (mg $L^{-1}$) | $C_{2,0}$[c] (mg $L^{-1}$) | $[\mathrm{DIN}]_0$ (mg $L^{-1}$) |
|---|---|---|---|---|
| $S_1, L_1$ | 10 | 0.374 | 1.325 | 1.699 |
| $S_2, L_2$ | 10 | 5.460 | 1.325 | 6.785 |

[a]S and L indicate that the test was conducted in the S and L streams, respectively. The morphological and hydraulic properties of these streams are shown in Table 1.
[b]Reported in the work of *Rutherford* [1994].
[c]The mean of the values reported by *Sjodin et al.* [1997].

### 3.3. Effect of Stream Morphology on DIN Transformations

[41] Figures 4a and 4b show how the dimensionless mass $\mu^*_{M,i}$ contained within the HZ of a low-gradient stream evolves with the dimensionless time $t^* = t\,K\,s_0\,C_z/L$ after an instantaneous in-stream pulse injection of ammonium and nitrate in the proportions RC = 0.282 and RC = 4.121, respectively. Tables 4 and 5 show the initial conditions and the reaction rates for the cases considered in Figures 4a (test $L_1$) and 4b (test $L_2$). In the definition of $t^*$ the characteristic time of transport is defined as the ratio between the hydraulic conductivity $K$ and a representative length ($L/s_0$) of the streamlines, while $C_z$ is the Chezy roughness coefficient, which influences the near-bed pressure distribution [*Marzadri et al.*, 2010]. For comparison, in Figure 4, we added the behavior of $\mu^*_M$ of a nonreactive tracer, which is obtained by setting $\chi_i(t) = 1$ and $C^*_{i,0} = 1$ in equation (22). Figures 5a and 5b are the same as Figures 4a and 4b for the S stream (see tests $S_1$ and $S_2$ in Tables 4 and 5).

[42] Comparison between the dimensionless mass of the $N_r$ species and of the tracer evidences the effect of biogeochemical processes on nutrient fate. Nitrification occurs between the downwelling area and the point along the streamline where oxygen concentration is depleted to the limit concentration ($C_{0,\mathrm{lim}} = 4$ mg $L^{-1}$ in our simulations). The remaining portion of the streamline up to the upwelling area is a zone of potential denitrification depending on nitrate availability. Therefore, the HZ can be in prevailing aerobic or anaerobic conditions depending on the distribution of the residence time $\tau_{\mathrm{up}}$. To help elucidate the part of the distribution of $\tau^*_{\mathrm{up}}$ in which $\tau^*_{\mathrm{lim}}$ is positioned, a few relevant $\alpha$ quartiles $\tau^*_{\mathrm{up},\alpha}$ of the residence time distribution are indicated in Figures 4a, 4b, 5a, and 5b with vertical dashed lines.

[43] The large variability of the travel time $\tau$, i.e., the time needed for a particle to travel from the downwelling area to a given position within the HZ, is visualized in Figure 6a, where we plot the isosurfaces $\tau$ for the L stream, and in Figure 6b, which shows the same quantity for the S stream. The surface with $\tau = \tau_{\mathrm{lim}}$, which envelops the HZ volume in aerobic conditions, is shown in inset 1 in both plots; the HZ volume external to this surface is in anaerobic conditions. The aerobic volume is shallower and occupies a smaller fraction of the hyporheic volume in the L stream (note that the two plots are not on the same scale). In both cases, the aerobic volume shows a complex shape originating in the downwelling area (pool), but that penetrates deeper into the HZ in the S streams. Figure 6a shows that the HZ of the L stream considered in the present study is in a prevailing anaerobic condition since more than 50% of the hyporheic volume is characterized by $\tau > \tau_{\mathrm{lim}}$. This is in line with experimental evidence that deeper flow paths with longer residence times show net denitrification [see, e.g., *Stonedahl et al.*, 2010].

[44] At early times (i.e., for $t^* < \tau^*_{\mathrm{lim}}$), the injected $NH_4^+$ is in the aerobic portion of the HZ where nitrification offsets the biomass consumption of $NO_3^-$. In this case, if the in-stream concentration of $NH_4^+$ is large enough, nitrification produces more $NO_3^-$ than the biomass can consume, such that the mass of $NO_3^-$ accumulates as shown in Figure 4b. However, when in-stream concentrations of $NH_4^+$ are

**Table 5.** Reaction Rate Coefficients at Reference Temperature of $T = 20°C$[a]

| Test | $T$(°C) | $z_d$ (m) | $K_R^{(20)}$[b] ($d^{-1}$) | $\varphi_R$[b] | $K_N^{(20)}$[c] ($d^{-1}$) | $\varphi_N$[c] | $K_D^{(20)}$[b] ($d^{-1}$) | $\varphi_D$[c] | $K_C^{(20)}$[d] ($d^{-1}$) | $\varphi_C$[d] |
|---|---|---|---|---|---|---|---|---|---|---|
| $S_1, S_2$ | 6 | 3 | 0.10 | 1.047 | 3.46 | 1.040 | 1.65 | 1.045 | 1.0 | 1.047 |
| $L_1, L_2$ | 6 | 30 | 0.10 | 1.047 | 3.46 | 1.040 | 1.65 | 1.045 | 1.0 | 1.047 |

[a] $T$ is the constant water temperature in the hyporheic zone, $z_d$ is the alluvium depth, $K_R^{(20)}$ is the reaction rate of biomass respiration, $K_N^{(20)}$ is the reaction rate of nitrification, $K_D^{(20)}$ is the reaction rate of denitrification, $K_C^{(20)}$ is the reaction rate of biomass consumption, and $\varphi_R$, $\varphi_N$, $\varphi_D$, and $\varphi_C$ are the dimensionless temperature coefficients for biomass respiration, nitrification, denitrification, and biomass consumption, respectively.
[b] Reported by *Rutherford* [1994].
[c] The mean of the values reported by *Sjodin et al.* [1997].
[d] One tenth of the value reported by *Dent and Henry* [1999].

low, nitrification alone is not sufficient to compensate the biomass consumption of $NO_3^-$, which therefore declines, as shown in Figure 4a. In both cases, nitrification reduces the mass of $NH_4^+$ at a rate that declines with time, converging, at the later times when the aerobic zone is free of ammonium, to the removal rate of a passive solute. Note that the position at which nitrification ceases (identified with the position where $\tau = \tau_{lim}$) changes with streamline, as shown in Figures 6a and 6b. From this point on, the residual $NH_4^+$ travels as a passive solute.

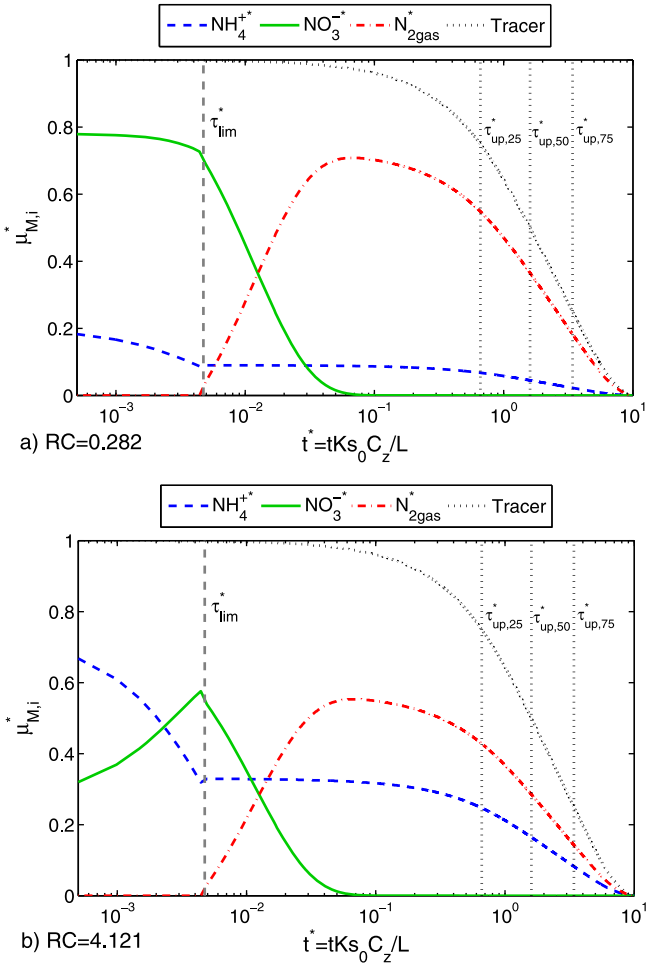


**Figure 4.** Dimensionless mass of dissolved inorganic nitrogen (DIN) species within the HZ as a function of dimensionless time in an L stream for (a) RC = 0.282 < 1 (test $L_1$) and (b) RC = 4.121 > 1 (test $L_2$) with a constant mean hyporheic temperature of 6°C.

[45] Which of these two cases prevails in a given period of time depends on local conditions, particularly on the time evolution of the in-stream concentration of $N_r$ species. The importance of biological processes in the aerobic portion of the HZ is highlighted by the sharp contrast between the evolution of the $N_r$ species and that of a passive tracer, which is depicted by a dotted line in Figures 4a and 4b. Almost all the tracer's mass (99.9%) is still within the HZ at times as large as $\tau_{lim}$, while $N_r$ species undergo biogeochemical transformations.

[46] $N_{gas}$ mirrors the behavior of $NO_3^-$, with its production increasing at the early stage of denitrification, when the decline of $NO_3^-$ is the fastest (see the red dash-dotted line in Figures 4a and 4b), successively increasing at a smaller rate, peaking at an intermediate time before declining to zero. The late decline of $NH_4^+$ is associated with its behavior as a passive tracer when nitrification ceases. Conversely, $NO_3^-$ is completely depleted by denitrification at $t^* \approx 0.05$, approximately when the production of $N_{gas}$ reaches its peak. Successively, the mass of $N_{gas}$ decreases within the HZ because of upwelling fluxes since denitrification does not occur because $NO_3^-$ has been consumed. Note that in formulating the biogeochemical model we implicitly assumed that $N_{gas}$ can leave the HZ only as a dissolved gas in the water emerging through the upwelling area.

[47] In the S stream, the residence time distribution is sharper and with a smaller median $\tau_{50}^*$ than for the L stream. While for the latter only 0.2% of the streamlines does not shift to anaerobic conditions somewhere between downwelling and upwelling areas (i.e., $\tau_{lim}^* \approx \tau_{up,0.2}^*$), this percentage increases to 25% for the former.

[48] At early times ($t^* < 0.074$) and for RC = 0.282, the injected $NH_4^+$ decreases slightly because of nitrification, whereas $NO_3^-$ remains nearly constant because of the compensating effects of nitrification and biomass uptake as a source and a sink of $NO_3^-$ (Figure 5a), respectively. Because of this, $NO_3^-$ seems to mimic the tracer behavior. On the other hand, for RC = 4.121 and for the same dimensionless time interval, the two $N_r$ species behave differently. As for the L stream, $NO_3^-$ increases with time, and $NH_4^+$ decreases faster than for RC = 0.282, whereas most of the injected mass of the tracer is still within the HZ, as shown by the passive solute curve. For larger times, $NH_4^+$ first decreases quickly because of the influence of both nitrification and upwelling fluxes, and then starting from $t^* = \tau_{lim}^* = 0.28$, it reduces to zero at a slower rate, as nitrification is inhibited in the anaerobic portion of the streamlines, and the decreasing rate is controlled exclusively by upwelling. In the anaerobic volume of the HZ, nitrate is converted to $N_{gas}$, and consequently, the mass of $NO_3^-$

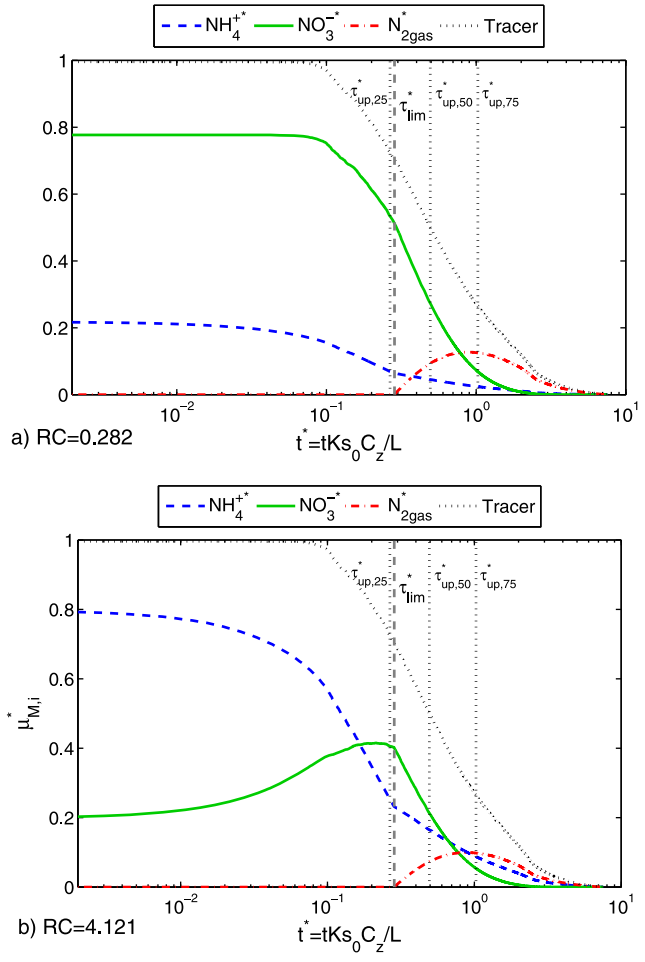


**Figure 5.** Dimensionless mass of DIN species at the upwelling area as a function of dimensionless time in an S stream for (a) RC = 0.282 < 1 (test $S_1$) and (b) RC = 4.121 > 1 (test $S_2$) with a constant mean hyporheic temperature of 6°C.

declines quickly to zero within the HZ, while that of $N_{gas}$ increases, peaking at an intermediate time (when the consumption rate of $NO_3^-$ is the largest observed) before declining to zero at later times.

[49] For a given RC, the dimensionless mass of $N_{gas}$ produced by denitrification is greater in the L stream than in the S stream (see Figures 4 and 5) because of its longer residence times, which results in the dominance of denitrification with respect to nitrification processes. In the L stream, aerobic processes are confined in a small portion of the hyporheic volume close to the downwelling area, and their effects vanish at times that are 1 order of magnitude smaller than the characteristic time of transport $\tau^*_{up,50}$ (50% of the streamlines have a residence time smaller than this value). On the other hand, small streams (see Figures 5a and 5b) are less effective in removing $NO_3^-$ because of prevailing aerobic conditions along the streamlines.

## 4. Discussion

[50] In section 3.1 we showed that our model is capable of predicting the emissions of $N_2O$ from seven reaches of the Kalamazoo River basin in southwestern Michigan, United States. This was possible because with the data published by *Beaulieu et al.* [2008, 2009] we were able to identify all the parameters of our model, particularly the geomorphological parameters. Unfortunately, in most cases, important pieces of information are lacking, which does not allow quantitative comparisons. However, there are cases in which we can at least compare qualitatively, in terms of evolution of the relevant processes, the results of our model with published experimental data. In section 4 we discuss some of these relevant cases.

[51] First, we observe that our model predicts denitrification processes in the HZ that are in qualitative agreement with the observations of *Pinay et al.* [2009] and *Zarnetske et al.* [2011] underneath gravel bars. In particular, *Zarnetske et al.* [2011] observed, in a well-instrumented gravel bar of Drift Creek in western Oregon, United States (49.975°N, 122.8259°W), a continuum between net nitrification and denitrification. This is in full agreement with our results, indicating that travel time distribution within the hyporheic sediments can be used as a proxy to separate volumes with net nitrification, where we observe production of $NO_3^-$, from volumes with net denitrification, where $NO_3^-$ is consumed and $N_2O$ increases. Moreover, both *Zarnetske et al.* [2011] and *Krause et al.* [2009] show nitrate and DO concentration patterns similar to our model, with DO always decreasing and nitrate production at short travel times, where nitrification occurs, replaced by consumption at long travel times, where denitrification takes over. However, *Krause et al.* [2009] data also show growth of the ammonium concentration with depth, which can be explained by the presence of sand and clay with high sorption-desorption capacity and by groundwater upwelling in some parts of their field site, where neither mechanism is included in our analysis.

[52] Similar to us, *Fernald et al.* [2006] observed ammonium concentration always decreasing within the HZ of a small gravel bed river in Oregon. They also suggest that S streams are chiefly characterized by oxidizing reactions. This is in line with our results in Figures 6a and 6b, which show the distribution of travel time for L and S rivers, respectively. Inset 1 in Figures 6a and 6b show that in S streams a larger fraction of the hyporheic volume is in aerobic conditions (i.e., the volume within which $\tau \leq \tau_{lim}$), which promote oxidation of $NH_4^+$ to $NO_3^-$ through nitrification.

[53] In field experiments, nitrate concentrations are typically measured along vertical profiles within the streambed sediment, and they are shown to vary with depth. These variations are consistent with the spatially variable redox conditions inherent in our modeling approach, as represented in Figure 7, which shows the distribution of $NO_3^-$ steady state concentration resulting from a continuous and constant in-stream $NO_3^-$ concentration of $C_{2,0} = 1.325$ mg $L^{-1}$ and RC = 0.282. In fact, as depth increases, the redox conditions and $NO_3^-$ concentrations change depending on the streamline that crosses that particular position. In addition, Figure 7 shows a complex three-dimensional pattern reflecting the control of bed topography on biogeochemical processes through the travel time distribution. In the corresponding pools, where downwelling zones are mainly localized, the nitrate concentration is close to the in-stream $NO_3^-$ concentration, while in the corresponding riffle, where upwelling

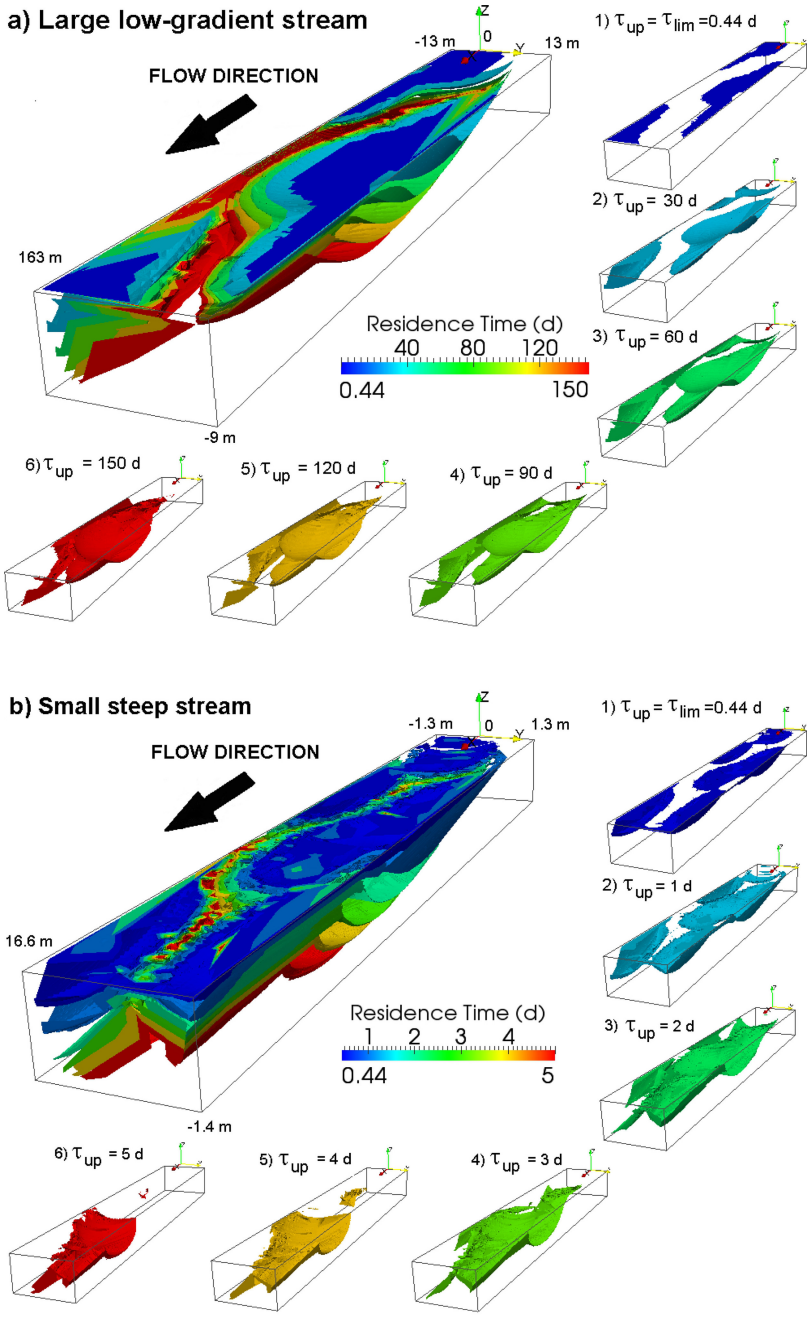


**Figure 6.** Pattern of variation of the residence time isosurface distribution in (a) the L stream and (b) the S stream.

zones are mainly localized, the nitrate concentration reflects the time that water spends within the streambed sediments. Moreover, we can distinctly observe the role of the hyporheic residence time on the prevailing aerobic or anaerobic conditions (see Figures 6b and 7). The residence time increases with depth because the length of the streamline up to that position increases with depth, and the prevailing anaerobic conditions promote denitrification processes that consume $NO_3^-$ and produce $N_{gas}$. Therefore, according to our model $NO_3^-$ concentrations may either increase or decrease along the streamline depending on redox conditions and in-stream $NH_4^+$ concentration. Figure 7 shows very complex spatial variations of nutrient distribution within the HZ. Thus, field measurements, which are typically based on a few spatially distributed point measurements, may not capture all the variability, which may affect microbial distribution and functions.

## 5. Conclusions

[54] We present a three-dimensional semianalytical process-based model, which predicts the fate of DIN species

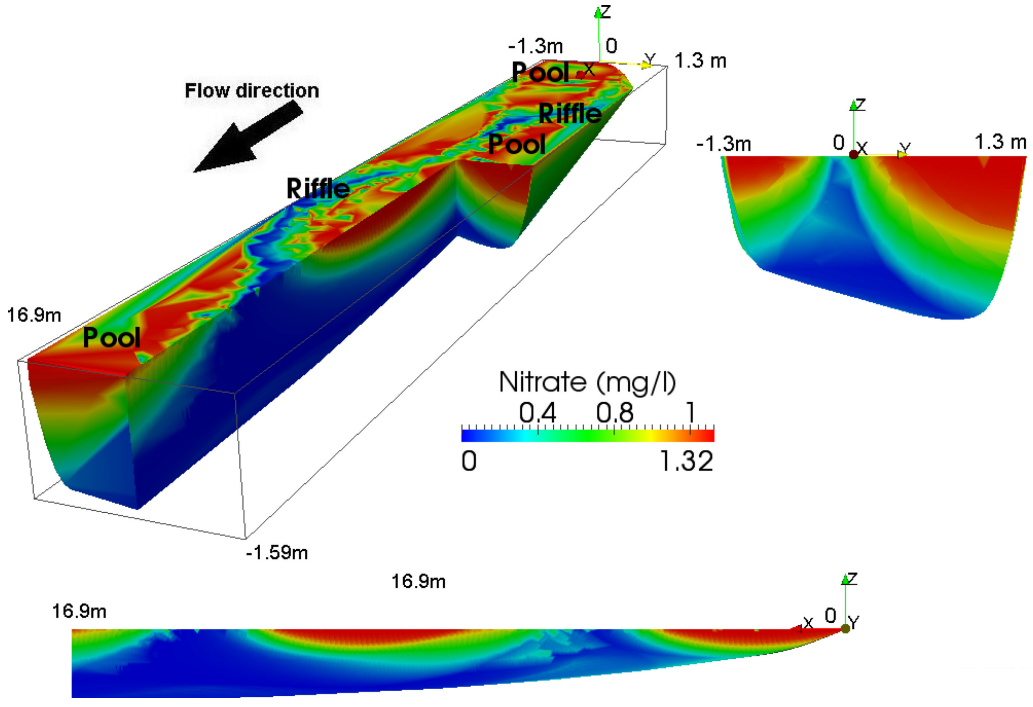


**Figure 7.** Pattern of variation of nitrate concentrations in the S stream initially rich with nitrate (RC = 0.282).

as they downwell in the HZ of a gravel bed river where DIN species undergo several biochemical transformations with time-dependent in-stream nitrogen concentrations. Comparison of model predictions of nitrous oxide emissions from seven natural streams with measured data shows good agreement. This shows that our model captures the main mechanisms leading to DIN transformation within the HZ of gravel bed rivers. To limit the complexity of the model and the number of parameters, we neglected mineralization and immobilization, DNRA reactions, and diffusion. However, these processes may be included, if needed, by taking advantage of the generality of the residence time approach that we adopted to develop our modeling framework. Furthermore, Monod reactions are simplified to first-order kinetics owing to the small DIN concentrations typically encountered in river systems, and dispersion is neglected as well. This allows us to derive analytical solutions of DIN transport and transformation. Under these hypotheses, we apply our model to analyze the response of a single alternate bar unit to an instantaneous solute injection, with the objective of providing a consistent framework for analyzing more complex cases with continuous injection of $N_r$ species in the stream water and highlighting the effect of streambed morphology on the $N_r$ cycle in riverine environments.

[55] The model shows complex concentration gradients, which differ from those of a nonreactive tracer within the HZ. Whereas ammonium mass always declines within the HZ at a rate depending on nitrification, nitrate mass may increase and/or decrease depending on the reciprocal strength of nitrification, biomass uptake, denitrification processes, and the ratio between the in-stream concentrations of nitrate and ammonium. These physical and biogeochemical gradients have important consequences on habitat quality and the type and location of the hyporheic fauna. The model captures the behavior of two important zones: an aerobic zone, which hosts nitrification processes, and an anaerobic zone, where denitrification reduces metabolic ready nitrate to $N_{gas}$, with the latter process removing nitrogen from the aquatic systems. The aerobic volume is a large portion of the HZ of S streams, whereas the anaerobic zone dominates in large, low-gradient streams. The prevailing aerobic conditions in the former rivers lead to lower emissions of $N_{gas}$ with respect to the latter at the bed form unit scale and for the same in-stream $N_r$ concentrations. However, at the river network–scale S streams may provide the larger contribution to the global removal of $NO_3^-$ and then potentially provide the larger contribution to $N_2O$ emissions because of their longer total length [*Rinaldo and Rodriguez-Iturbe*, 1996; *Tonina and Buffington*, 2009]. S streams are also important sources of nitrate when RC $>$ 1, even though this is a less common circumstance.

[56] **Acknowledgments.** This research was partially supported by the EU project AQUATERRA (contract 505428-GOCE), by the project "Analysis of flow and transport processes at the hillslope scale" (2008A7EBA3) funded by the Italian Ministry of Education, Universities and Research, and by the postdoc 2006 grant (project "Flussi Iporreici") of the autonomous province of Trento (Italy). We thank the three anonymous reviewers and the Associated Editor for the valuable comments.

## References

Arango, C. P., and J. L. Tank (2008), Land use influences the spatiotemporal controls of nitrification and denitrification in headwater streams, *J. North Am. Benthol. Soc.*, *27*(1), 90–107.

Bailey, J. E., and D. F. Ollis (1977), *Biochemical Engineering Fundamentals*, McGraw-Hill, New York.

Basu, N. B., et al. (2010), Nutrient loads exported from managed catchments reveal emergent biogeochemical stationarity, *Geophys. Res. Lett.*, *37*, L23404, doi:10.1029/2010GL045168.

Beaulieu, J. J., C. P. Arango, S. K. Hamilton, and J. L. Tank (2008), The production and emission of nitrous oxide from headwater in the midwestern United States, *Global Change Biol.*, *14*, 878–894.

Beaulieu, J. J., C. P. Arango, and J. L. Tank (2009), The effects of season and agriculture on nitrous oxide production in headwater streams, *J. Environ. Qual.*, *38*, 637–646.

Beaulieu, J. J., et al. (2011), Nitrous oxide emission from denitrification in stream and river networks, *Proc. Natl. Acad. Sci. U. S. A.*, *108*(1), 214–219.

Bencala, K. E., and R. A. Walters (1983), Simulation of solute transport in a mountain pool-and-riffle stream: A transient storage model, *Water Resour. Res.*, *19*, 718–724, doi:10.1029/WR019i003p00718.

Bernot, M. J., and W. K. Dodds (2005), Nitrogen retention, removal, and saturation in lotic ecosystems, *Ecosystem*, *8*, 442–453.

Boano, F., A. Demaria, R. Revelli, and L. Ridolfi (2010), Biogeochemical zonation due to intrameander hyporheic flow, *Water Resour. Res.*, *46*, W02511, doi:10.1029/2008WR007583.

Bölke, J. K., and J. M. Denver (1995), Combined use of groundwater dating, chemical, and isotopic analyses to resolve the history and fate of nitrate contamination in two agricultural watersheds, Atlantic coastal plain, Maryland, *Water Resour. Res.*, *31*, 2319–2339, doi:10.1029/95WR01584.

Buss, S. R., M. Rivett, P. Morgan, and C. D. Bemment (2005), Attenuation of nitrate in the sub-surface environment, science report SC030155/SR2, Environ. Agency, Bristol, U. K.

Butturini, A., T. J. Battin, and F. Sabater (2000), Nitrification in stream sediment biofilms: The role of ammonium concentration and DOC quality, *Water Res.*, *34*(2), 629–639.

Cardenas, M. B., and J. L. Wilson (2007), Exchange across a sedimentwater interface with ambient groundwater discharge, *J. Hydrol.*, *346*, 69–80.

Cardenas, M. B., P. L. M. Cook, H. Jiang, and P. Traykovski (2008), Constraining denitrification in permeable wave-influenced marine sediment using linked hydrodynamic and biogeochemical modeling, *Earth Planet. Sci. Lett.*, *275*, 127–137.

Colombini, M., G. Seminara, and M. Tubino (1987), Finite-amplitude alternate bars, *J. Fluid Mech.*, *181*, 213–232.

Cooper, A. B. (1984), Activities of benthic nitrifiers in streams and their role in oxygen consumption, *Microb. Ecol.*, *10*(4), 317–334.

Cooper, C. M. (1993), Biological effects of agriculturally-derived surface water pollutants on aquatic systems: A review, *J. Environ. Qual.*, *22*, 402–408.

Cvetkovic, V., and G. Dagan (1994), Transport of kinetically sorbing solute by steady random velocity in heterogeneous porous formation, *J. Fluid Mech.*, *265*, 189–215.

Dagan, G. (1989), *Flow and Transport in Porous Formations*, Springer, New York.

Dagan, G., V. Cvetkovic, and A. M. Shapiro (1992), A solute flux approach to transport in heterogeneous formations: 1. The general framework, *Water Resour. Res.*, *28*, 1369–1376, doi:10.1029/91WR03086.

Demmy, G., S. Berglund, and W. Graham (1999), Injection mode implications for solute transport in porous media: Analysis in a stochastic Lagrangian framework, *Water Resour. Res.*, *35*, 1965–1973, doi:10.1029/1999WR900027.

Dent, C. L., and J. C. Henry (1999), Modelling nutrient-periphyton dynamics in streams with surface-subsurface exchange, *Ecological Modell.*, *122*, 97–116.

Duff, J. H., and F. Triska (2000), Nitrogen biogeochemistry and surface-subsurface exchange in streams, in *Streams and Ground Waters*, edited by J. Jones and P. Muholland, pp. 197–220, Academic, San Diego, Calif.

Elliott, A. H., and N. H. Brooks (1997), Transfer of nonsorbing solutes to a streambed with bedforms: Laboratory experiments, *Water Resour. Res.*, *33*, 137–151, doi:10.1029/96WR02783.

Fernald, A. G., D. H. Landers, and P. J. Wigington Jr. (2006), Water quality changes in hyporheic flow paths between a large gravel bed river and off-channel alcoves in Oregon, USA, *River Res. Appl.*, *22*(10), 1111–1124.

Freeze, A. R., and J. A. Cherry (1979), *Groundwater*, Prentice-Hall, Englewood Cliffs, N. J.

Galloway, J. N., et al. (2004), Nitrogen cycles: Past, present, and future, *Biogeochemistry*, *70*(2), 153–226.

Galloway, J. N., A. R. Townsend, J. W. Erisman, M. Bekunda, Z. Cai, J. R. Freney, L. A. Martinelli, S. P. Seitzinger, and M. A. Sutton (2008), Transformation of the nitrogen cycle: Recent trends, questions and potential solutions, *Science*, *320*, 889–892.

Green, C. T., J. K. Böhlke, B. A. Bekins, and S. P. Phillips (2010), Mixing effects on apparent reaction rates and isotope fractionation during denitrification in a heterogeneous aquifer, *Water Resour. Res.*, *46*, W08525, doi:10.1029/2009WR008903.

Hantush, M. M. (2005), Modeling stream-aquifer interactions with linear response functions, *J. Hydrol.*, *311*, 59–79.

Hantush, M. M. (2007), Modeling nitrogen-carbon cycling and oxygen consumption in bottom sediments, *Adv. Water Resour.*, *30*(1), 59–79.

Harvey, J. W., and K. E. Bencala (1993), Effect of streambed topography on surface-subsurface water exchange in mountain catchments, *Water Resour. Res.*, *29*, 89–98, doi:10.1029/92WR01960.

Hemond, H. F., and A. P. Duran (1989), Fluxes of $N_2O$ at the sediment-water and water-atmosphere boundaries of a nitrogen-rich river, *Water Resour. Res.*, *25*, 839–846, doi:10.1029/WR025i005p00839.

Huttel, M., W. Zibis, and S. Forster (1996), Flow-induced uptake of particulate matter in permeable sediments, *Limnol. Oceanogr.*, *41*(2), 309–322.

Kelso, B. H. L., R. V. Smith, and R. J. Laughlin (1999), Effects of carbon substrate on nitrite accumulation in freshwater sediments, *Appl. Environ. Microbiol.*, *65*, 61–66.

Kendall, C., E. M. Elliott, and S. D. Wankel (2007), Tracing anthropogenic inputs of nitrogen to ecosystems, in *Stable Isotopes in Ecology and Environmental Science*, 2nd ed., edited by R. Michener and K. Lajtha, pp. 375–449, Blackwell, Malden, Mass.

Kjellin, J., S. Hallin, and A. Wörman (2007), Spatial variations in denitrification activity in wetland sediments explained by hydrology and denitrifying community structure, *Water Res.*, *41*(20), 4710–4720.

Krause, S., L. Heathwaite, A. Binley, and P. Keenan (2009), Nitrate concentration changes at the groundwater-surface water interface of a small Cumbrian river, *Hydrol. Processes*, *23*(15), 2195–2211.

Kreft, A., and A. Zuber (1978), On the physical meaning of the dispersion equation and its solutions for different initial and boundary conditions, *Chem. Eng. Sci.*, *33*(11), 1471–1480.

Lewis, D. B., N. B. Grimm, T. K. Harms, and J. D. Schade (2007), Subsystems, flowpaths, and the spatial variability of nitrogen in a fluvial ecosystem, *Landscape Ecol.*, *22*(6), 911–924.

Marion, A., M. Bellinello, I. Guymer, and A. I. Packman (2002), Effect of bed form geometry on the penetration of nonreactive solutes into a streambed, *Water Resour. Res.*, *38*(10), 1209, doi:10.1029/2001WR000264.

Marzadri, A., D. Tonina, A. Bellin, G. Vignoli, and M. Tubino (2010), Semianalytical analysis of hyporheic flow induced by alternate bars, *Water Resour. Res.*, *46*, W07531, doi:10.1029/2009WR008285.

McLaren, A. D. (1976), Rate constants for nitrification and denitrification in soils, *Radiat. Environ. Biophys.*, *13*(1), 43–48.

Mulholland, P. J., and D. L. DeAngelis (2000), Surface-subsurface exchange and nutrient spiraling, in *Streams and Ground Waters*, edited by J. Jones and P. Muholland, pp. 149–166, Academic, San Diego, Calif.

Newbold, J. D., R. V. O'Neill, J. W. Elwood, and W. VanWinkle (2000), Nutrient spiralling in streams: Implications for nutrient limitation and invertebrate activity, *Am. Nat.*, *120*(5), 628–652.

Packman, A. I., and K. E. Bencala (2000), Modeling surface-subsurface hydrologic interactions, in *Streams and Ground Waters*, edited by J. Jones and P. Muholland, pp. 45–80, Academic, San Diego, Calif.

Packman, A. I., and N. H. Brooks (2001), Hyporheic exchange of solutes and colloids with moving bed forms, *Water Resour. Res.*, *37*, 2591–2605, doi:10.1029/2001WR000477.

Peterson, B., et al. (2001), Control of nitrogen export from watershed by headwater streams, *Nature*, *292*, 86–89.

Pinay, G., T. C. O'Keefe, R. T. Edwards, and R. J. Naiman (2009), Nitrate removal in the hyporheic zone of a salmon river in Alaska, *River Res. Appl.*, *25*(4), 367–375.

Potter, J. D., W. H. McDowell, J. L. Merriam, B. J. Peterson, and S. M. Thomas (2010), Denitrification and total nitrate uptake in streams of a tropical landscape, *Ecol. Appl.*, *20*(8), 2104–2115.

Puckett, L. J., C. Zamora, H. Essaid, J. T. Wilson, H. M. Johnson, M. J. Brayton, and J. R. Vogel (2008), Transport and fate of nitrate at the ground-water/surface-water interface, *J. Environ. Qual.*, *37*, 1034–1050.

Rinaldo, A., and I. Rodriguez-Iturbe (1996), Geomorphological theory of the hydrologic response, *Hydrol. Processes*, *10*(6), 803–829.

Rubin, Y. (2003), *Applied Stochastic Hydrogeology*, Oxford Univ. Press, New York.

Rutherford, J. C. (1994), *River Mixing*, John Wiley, Chichester, U. K.

Rutherford, J. C., J. D. Boyle, A. H. Elliott, T. V. J. Hatherell, and T. W. Chiu (1995), Modeling benthic oxygen uptake by pumping, *J. Environ. Eng.*, *121*(1), 84–95.

Seitzinger, S., C. Kroeze, and R. Styles (2000), Global distribution of $N_2O$ emissions from aquatic systems: Natural emissions and anthropogenic effects, *Chemosphere Global Change Sci.*, *2*, 267–279.

Shaffer, M. J., K. Lasnik, X. Ou, and R. Flynn (2001), NLEAP internet tools for estimating $NO_3^-$ N leaching and $N_2O$ emissions, in *Modeling Carbon and Nitrogen Dynamics for Soil Management*, edited by S. Hansen, M. J. Shaffer and L. Ma, pp. 401–426, A. F. Lewis, Boca Raton, Fla.

Shapiro, A. M., and V. Cvetkovic (1988), Stochastic analysis of solute arrival time in heterogeneous porous media, *Water Resour. Res.*, *24*, 1711–1718, doi:10.1029/WR024i010p01711.

Sheibley, R. V., A. P. Jackman, J. H. Duff, and F. J. Triska (2003), Numerical modeling of coupled nitrification-denitrification in sediment perfusion cores from the hyporheic zone of the Shingobee River, MN, *Adv. Water Resour.*, *26*(9), 977–987.

Sjodin, A. L., W. M. Lewis, and J. F. Saunders III (1997), Denitrification as a component of the nitrogen budget for a large plains river, *Biogeochemistry*, *39*(3), 327–342.

Smil, V. (1999), Long-range perspectives on inorganic fertilizers in global agriculture, technical report, Int. Fert. Dev. Cent., Muscle Shoals, Ala.

Sobczak, W., S. Findlay, and S. Dye (2003), Relationships between DOC bioavailability and nitrate removal in an upland stream: An experimental approach, *Biogeochemistry*, *62*(3), 309–327.

Spalding, R. F., and M. E. Exner (1993), Occurrence of nitrate in groundwater a review, *J. Environ. Qual.*, *22*(3), 392–402.

Stonedahl, S. H., J. W. Harvey, A. Wörman, M. Salehin, and A. I. Packman (2010), A multiscale model for integrating hyporheic exchange from ripples to meanders, *Water Resour. Res.*, *46*, W12539, doi:10.1029/2009WR008865.

Sylvia, D. M., J. J. Fuhrmann, P. G. Hartel, and D. A. Zuberer (2005), *Principles and Applications of Soil Microbiology*, Prentice Hall, Upper Saddle River, N. J.

Tesoriero, A. J., H. Liebscher, and S. E. Cox (2000), Mechanism and rate of denitrification in an agricultural watershed: Electron and mass balance along groundwater flow paths, *Water Resour. Res.*, *36*, 1545–1559, doi:10.1029/2000WR900035.

Tiedje, J. M. (1988), Ecology of denitrification and dissimilatory nitrate reduction to ammonia, in *Biology of Anaerobic Microrganisms*, pp. 179–244, John Wiley, New York.

Tonina, D., and J. M. Buffington (2007), Hyporheic exchange in gravel bed rivers with pool-riffle morphology: Laboratory experiment and three-dimensional modeling, *Water Resour. Res.*, *43*, W01421, doi:10.1029/2005WR004328.

Tonina, D., and J. M. Buffington (2009), Hyporheic exchange in mountain rivers I: Mechanics and environmental effects, *Geogr. Compass*, *3*(3), 1063–1086.

Triska, F. K., J. H. Duff, and R. J. Avanzino (1993), The role of water exchange between a stream channel and its hyporheic zone in nitrogen cycling at the terrestrial-aquatic interface, *Hydrobiologia*, *251*(1–3), 167–184.

Triska, F. K., A. P. Jackman, J. H. Duff, and R. J. Avanzino (1994), Ammonium sorption to channel and riparian sediments: A transient storage pool for dissolved inorganic nitrogen, *Biogeochemistry*, *26*(2), 67–83.

van Genuchten, M. T. (1981), Analytical solutions for chemical transport with simultaneous adsorption, zero order production and first order decay, *J. Hydrol.*, *49*(3–4), 213–233.

Wondzell, S. M., and F. J. Swanson (1996), Seasonal and storm dynamics of the hyporheic zone of 4-th order mountain stream. II: Nitrogen cycling, *J. North Am. Benthol. Soc.*, *15*(1), 20–34.

Zarnetske, J. P., R. Haggerty, S. M. Wondzell, and M. A. Baker (2011), Dynamics of nitrate production and removal as a function of residence time in the hyporheic zone, *J. Geophys. Res.*, *116*, G01025, doi:10.1029/2010JG001356.

A. Bellin and A. Marzadri, Department of Civil and Environmental Engineering, University of Trento, Via Mesiano 77, I-38123 Trento, Italy. (alberto.bellin@ing.unitn.it; alessandra.marzadri@ing.unitn.it)

D. Tonina, Center for Ecohydraulics Research, University of Idaho, 322 E. Front St., Ste. 340, Boise, ID 83702, USA. (dtonina@uidaho.edu)